Cell

Crystal Structure of a 70S Ribosome-tRNA Complex Reveals Functional Interactions and Rearrangements

Andrei Korostelev,[1] Sergei Trakhanov,[1] Martin Laurberg,[1] and Harry F. Noller[1,*]
[1] Center for Molecular Biology of RNA and Department of Molecular, Cell and Developmental Biology, University of California, Santa Cruz, Santa Cruz, CA 95064, USA
*Contact: harry@nuvolari.ucsc.edu
DOI 10.1016/j.cell.2006.08.032

SUMMARY

Our understanding of the mechanism of protein synthesis has undergone rapid progress in recent years as a result of low-resolution X-ray and cryo-EM structures of ribosome functional complexes and high-resolution structures of ribosomal subunits and vacant ribosomes. Here, we present the crystal structure of the *Thermus thermophilus* 70S ribosome containing a model mRNA and two tRNAs at 3.7 Å resolution. Many structural details of the interactions between the ribosome, tRNA, and mRNA in the P and E sites and the ways in which tRNA structure is distorted by its interactions with the ribosome are seen. Differences between the conformations of vacant and tRNA-bound 70S ribosomes suggest an induced fit of the ribosome structure in response to tRNA binding, including significant changes in the peptidyl-transferase catalytic site.

INTRODUCTION

Ribosomes are the ribonucleoprotein complexes responsible for protein synthesis in all living cells. Detailed knowledge of their molecular structure and the ways in which they interact with mRNA, tRNA, and other functional ligands is essential for understanding the mechanism of this central process of gene expression. The smallest ribosomes, from bacteria and archaea, have molecular weights of about 2.5 MDa and are composed of about 60% RNA and 40% protein. Their small (30S) subunits contain 16S rRNA (~1500 nucleotides) and about 20 proteins; their large (50S) subunits contain 23S rRNA (~2900 nucleotides), 5S rRNA (~120 nucleotides), and more than 30 proteins. Unlike other polymerases, the mechanism of action of ribosomes appears to be based on their RNA (Green and Noller, 1997; Nissen et al., 2000; Noller et al., 1992). The formidable structural complexity of the ribosome is compounded by its structural dynamics, which underlie its functional capabilities. An important challenge, therefore, is to understand the structure of the ribosome not only at high resolution but in different complexes representing its many different functional states.

In recent years, rapid progress has been made in the determination of ribosome structures. Cryo-EM reconstructions of ribosomes and many functional ribosome complexes have provided low-resolution representations of the ribosome trapped in different states of the translational process (Agrawal et al., 1999; Frank and Agrawal, 2000; Gao et al., 2003; Stark et al., 2000). These studies have provided the first indications of large-scale molecular movements such as relative rotation of the two subunits during translocation (Frank and Agrawal, 2000). Until recently, the most detailed views of the ribosome came from all-atom crystal structures of the isolated 30S and 50S subunits from *Thermus thermophilus, Haloarcula marismortui*, and *Deinococcus radiodurans* (Ban et al., 2000; Harms et al., 2001; Wimberly et al., 2000), which in some cases were cocrystals containing model tRNAs and mRNAs (Ogle et al., 2001, 2002; Schmeing et al., 2002, 2003), antibiotics (Brodersen et al., 2000; Hansen et al., 2002; Pioletti et al., 2001), and translation factors (Pioletti et al., 2001; Wilson et al., 2005). These structures have not only revealed the three-dimensional structures of the rRNAs, ribosomal proteins, and their mutual interactions but have also led to proposals for the mechanisms of aminoacyl-tRNA selection, catalysis of peptide bond formation, and the modes of action of many antibiotics. However, a complete understanding of protein synthesis requires knowledge of the structure of functional complexes of the whole ribosome, its true biological context.

The first crystal structures of complete ribosomes, from *T. thermophilus* 70S complexes, provided a description of the interactions between tRNA and the ribosome in the A, P, and E sites and identified the molecular components of the intersubunit bridges and the path of the mRNA (Yusupov et al., 2001; Yusupova et al., 2001). The structure of a 70S complex containing a model threonyl-tRNA synthetase mRNA and tRNAs bound to the A and P sites has shown how structure in the 5′ leader of the mRNA is able to regulate initiation of translation (Jenner et al., 2005). More recently, the structures of complexes containing the

release factors RF1 and RF2 have provided insight into the mechanism of translational termination (Petry et al., 2005). So far, the structures of these 70S complexes have been limited to resolutions of between 5.5 and 7 Å, preventing a more complete understanding of the molecular basis of the interactions between the ribosome and its main functional ligands as well as the ways in which they perturb each other's structures during translation. In a recent landmark paper, the structures of two conformational states of the *Escherichia coli* 70S ribosome were solved at 3.5 Å resolution, representing the most detailed view of the complete ribosome obtained so far and providing new information about the structural basis of ribosome dynamics (Schuwirth et al., 2005). The impact of these structures on our understanding of protein synthesis is nevertheless limited by the absence of mRNA and tRNA. Here, we report the crystal structure of a complex of the *T. thermophilus* 70S ribosome containing a model mRNA and two tRNAs, bound to the P and E sites, at 3.7 Å resolution. The improved resolution enables visualization of the nature of molecular interactions between the ribosome, mRNA, and full-length tRNAs for the first time. Moreover, it shows how the conformations of both the tRNAs and the ribosome are perturbed by formation of the tRNA-ribosome complex.

RESULTS AND DISCUSSION

Structure Determination

A complex of the *Thermus thermophilus* 70S ribosome containing a 10 nucleotide model mRNA and two tRNAs was crystallized in a new crystal form (Yusupov et al., 2001; see also Figure S2 in the Supplemental Data available with this article online), belonging to the I422 space group, with unit-cell dimensions a = b = 507.8 Å, c = 689.5 Å, that diffracts to 3.7 Å (Table 1). Shortening of the c axis by ~110 Å relative to the previous crystal form (Yusupov et al., 2001) is mainly due to rearrangement of one of the lattice contacts, in which the stalks of 5S rRNA symmetry mates run parallel to each other rather than stacking coaxially. An *E. coli* $tRNA^{Phe}$ was bound to the P site, and an endogenous tRNA (most likely a heterogeneous mixture of *T. thermophilus* tRNAs) occupied the E site.

Structure determination was done using the molecular replacement method, followed by rigid-body refinement using successively finer rigid-body groups. Finally, alternating rounds of reciprocal- and real-space (Korostelev et al., 2002) refinement, interspersed with manual refitting, were used, resulting in a value for R_{free} of 0.35 (see Experimental Procedures). The positions of RNA bases, riboses, and phosphates and the main chains of the proteins could be assigned to features of the electron density map (Figure 1C; Figures 2A–2C; Figure S1), with the exception of proteins L7/L12, L10, L11, L31, and L33; positions 55-160 of L1; the 3′ end of the mRNA including the A codon; and the very 5′ and 3′ ends of 16S rRNA, which were disordered.

Table 1. Summary of Crystallographic Data and Refinement

Data Statistics	
Unit-cell dimensions, Å	a = b = 507.8, c = 689.5
Resolution, Å	3.7–75 (3.8)
Number of unique reflections	465,894 (33,259)
Completeness, %	99.3 (96.6)
Multiplicity	5.4 (4.1)
Mean I/σ(I)	3.0 (1.5)
R_{pim}	0.149 (0.467)
Refinement Statistics	
Resolution, Å	3.7–30.0
Test-set (free) reflections, %	2.5
R/R_{free} (CNS)	0.358/0.366
R/R_{free} (REFMAC)	0.346/0.347
Deviation from ideal bond lengths, Å	0.013
Deviation from ideal bond angles, °	1.36

All measured reflections were used in refinements with CNS and REFMAC. R_{pim} denotes the precision-indicating merging R factor (Weiss, 2001). Statistics for the highest resolution shell are given in parentheses.

The 70S P Site

The roles of the P site are to hold the peptidyl-tRNA tightly to prevent loss of the nascent chain, to maintain the correct translational reading frame when the A site is vacant, and to bind the initiator tRNA during initiation of protein synthesis. In our complex, an *E. coli* $tRNA^{Phe}$ is held in position by numerous interactions with 16S and 23S rRNA and three ribosomal proteins, in addition to base pairing with a UUC codon (Figures 1A and 1B; Table S1). In the 30S P site, the main contacts with the anticodon stem-loop (ASL) and codon are made by 16S rRNA, bolstered by interactions with the C-terminal tail of protein S13, as described below. In the 50S P site, the minor groove of the P-tRNA D stem rests on the minor groove of helix 69 of 23S rRNA. The P-tRNA elbow contacts an extended β hairpin of protein L5. Nucleotide 2 of its acceptor stem interacts with the P stem (helix 80) of 23S rRNA. The N-terminal end of protein L27, which approaches the end of the acceptor stem, is well ordered in our electron density map beginning only at position 9; its N-terminal tail is disordered. The β hairpin at position 82 of protein L16 approaches within 10 Å of the major-groove face of the acceptor stem of P-tRNA at positions 2 and 64; although not in direct contact, its position suggests that it could interact transiently with the tRNA as it moves between the A and P sites.

Ribosomal interactions with tRNA in the 30S P site contrast sharply with those in the 30S A site, which, in keeping

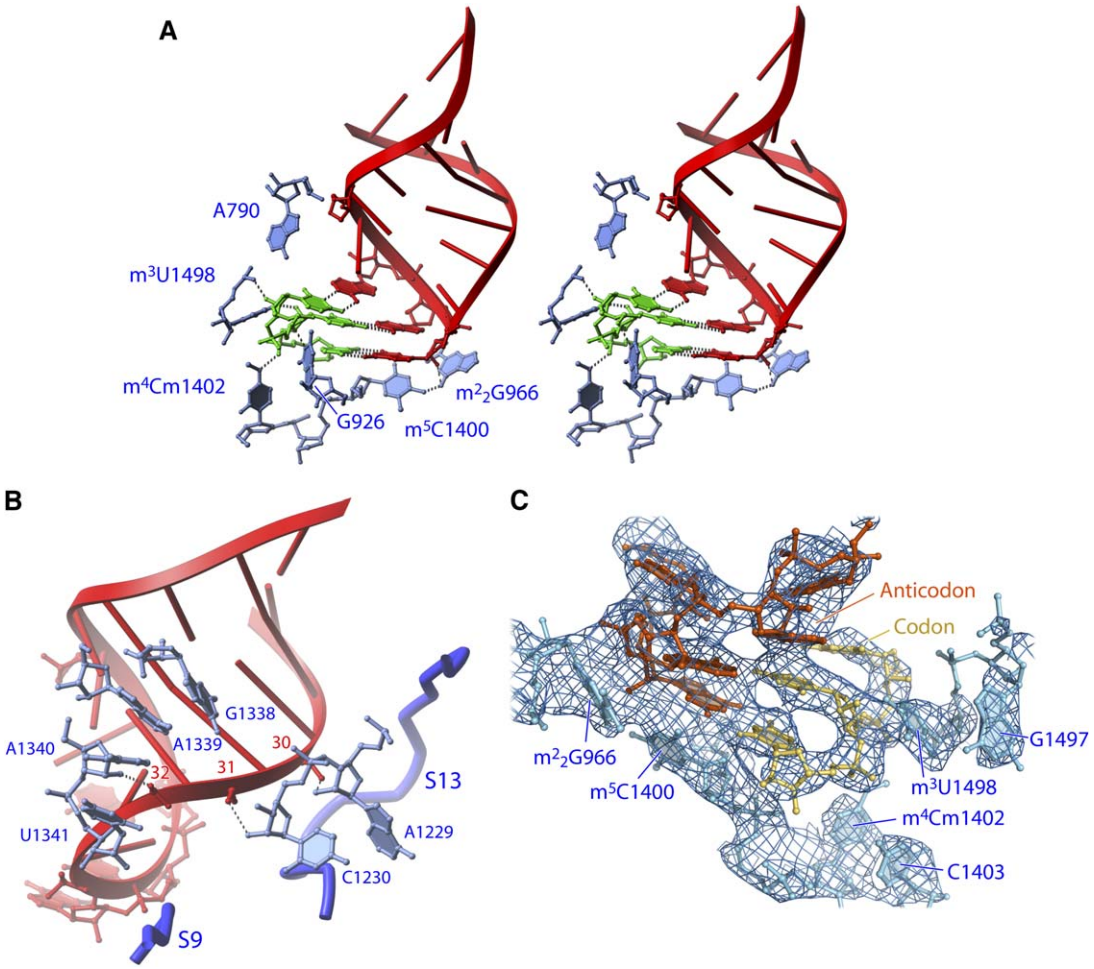

Figure 1. The 30S Subunit P Site

(A) Stereo diagram showing details of interactions between 16S rRNA and the codon-anticodon helix.

(B) Interactions between the anticodon stem and the ribosome.

(C) Electron density map of the 30S P site (composite omit map contoured at 2.0σ) showing the codon (yellow), anticodon (orange), and surrounding features of 16S rRNA (cyan).

with its role in selecting the correct aminoacyl-tRNA, contacts the tRNA and mRNA with only four nucleotides of 16S rRNA, three of which fit precisely into the minor groove of the codon-anticodon helix (Ogle et al., 2001). In the P site, eight nucleotides of the P site codon and tRNA anticodon stem-loop (ASL) are fixed in position by interactions with ten nucleotides of 16S rRNA, which include four of its eleven posttranscriptionally methylated nucleotides (Guymon et al., 2006). In *T. thermophilus* ribosomes, these interactions are bolstered by interactions with the extended C-terminal tail of protein S13. Four universally conserved nucleotides contact the P codon backbone of mRNA, forming H bonds with all three codon nucleotides.

Phosphate 1 of the P codon is H bonded to the N1 and N2 positions of G926. m^3U1498 packs against the ribose-phosphate backbone of nucleotides 1 and 2 of the P codon, making an H bond from its O4 position to the 2′ hydroxyl of codon nucleotide 2. The phosphate group of codon nucleotide 3 H bonds with the 4-methylamino group of m^4Cm1402. No contacts are made between the ribosome and the P codon bases. In addition to base pairing with the P codon, the anticodon of the P site tRNA is buttressed by stacking with base m^5C1400 on its wobble base (G34), as predicted more than 20 years ago by Ofengand, Zimmermann, and coworkers (Prince et al., 1982), and by packing of $m^2{}_2$G966 against ribose 34 (Figure 1B). The sole protein contacts are with the highly basic C-terminal tail of protein S13, at phosphates 31 and 36 (Figure 1B). The extensive packing of 16S rRNA around the third base pair contrasts with what is observed for the 30S A site, where minimal interactions explain the prevalence of third-position wobble in the genetic code (Ogle et al., 2001). In contrast, during translational initiation in the 30S P site, initiator $tRNA^{fMet}$ can recognize AUG, GUG, or UUG as methionine start

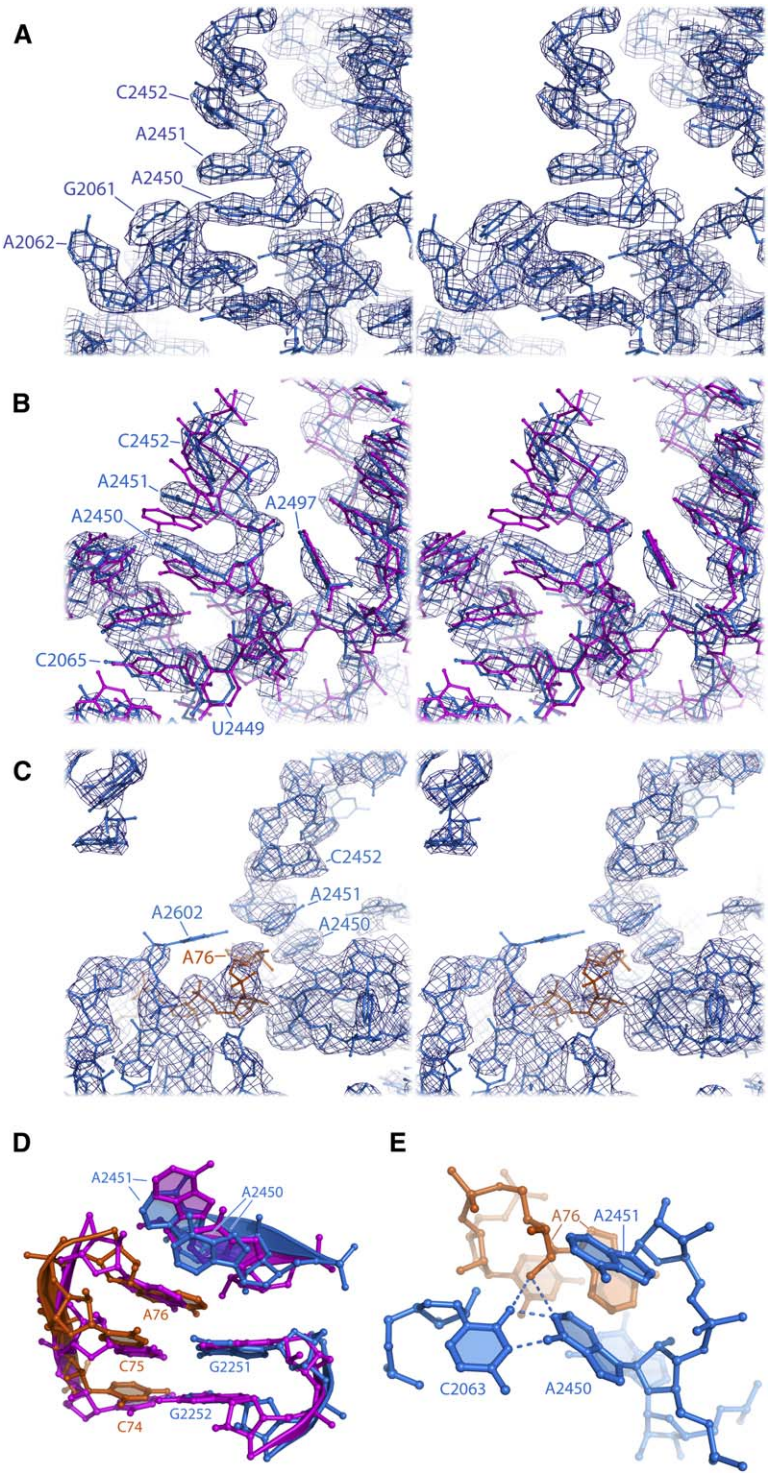

Figure 2. The Peptidyl-Transferase P Site

(A) Stereoview of the electron density map showing fitting of 23S rRNA features in the peptidyl-transferase P site (composite omit map contoured at 1.8σ).

(B) Stereoview of superposition of 23S rRNA from the *H. marismortui* 50S complex (PDB ID code 1QVG) bound with a CCA oligonucleotide (Schmeing et al., 2003) on the *T. thermophilus* 70S complex (blue) in the context of the electron density map, showing differences in the positions of A2450 and A2451.

(C) Stereoview of the *T. thermophilus* 70S complex showing fitting of 23S rRNA (blue) and tRNA (orange) features in the electron density map.

(D) Superposition of structures in (B) in a view showing movement of A2450 and A2451 of 23S rRNA (blue) and A76 of P-tRNA (orange) toward each other in the 70S complex, relative to the 50S complex (magenta).

(E) Detailed view showing juxtaposition of ribose 76 of P-tRNA (orange) with the protonated C2063-A2450 base pair and A2451 of 23S rRNA (blue).

codons—i.e., wobble is tolerated in the first rather than in the third position. The contrasting architectures of the 30S A and P sites may underlie their different rules for codon-anticodon pairing.

Interactions with the anticodon stem involve both backbone and minor-groove interactions, focused on nucleotides 30 and 31 (Figure 1B). Extensive interactions, including H bonding and van der Waals packing, are made between the backbones of nucleotides 1229, 1230, and 1341 and the tRNA (Figure 1B). In the same region, bases G1338 and A1339 are positioned in the minor groove of the anticodon stem, poised to make potential type II and

type I A-minor interactions with the 29-41 and 30-40 base pairs, which would require movement of this region of the head by ~1.5 Å. These interactions are believed to mediate discrimination of initiator tRNA during formation of the 30S initiation complex (Dallas and Noller, 2001; Lancaster and Noller, 2005). In their analysis of the structure of the 70S ribosome, Schuwirth et al. (2005) pointed out that there is a structural barrier to movement of tRNA from the P to E sites, created by the ridge containing G1338 and A1339 and the 790 loop, which are separated by only ~13 Å in their structures. This barrier is maintained in our structure, where the gap is reduced by only a fraction of an angstrom, requiring movement of the head of the 30S subunit to permit translocation, as proposed by Schuwirth et al. The positions of the 16S rRNA P site nucleotides in the vacant ribosome superimpose upon those in the tRNA-containing complex around the codon-anticodon interaction (with the exception of the flipped $m^2{}_2$G966), but the nucleotides that contact the anticodon stem are displaced by several angstroms due to movement of the head of the 30S subunit. The observed 16S rRNA-tRNA contacts are in agreement with chemical probing studies in which binding of tRNA to the P site protected G926, m^2G966, G1338, A1339, and C1400 from attack by the base-specific probes kethoxal and dimethyl sulfate (Moazed and Noller, 1986, 1991); modification of three of these bases (G926, m^2G966, and G1338) was shown to interfere with binding of tRNA to the *E. coli* 30S P site (von Ahsen and Noller, 1995).

The Peptidyl-Transferase Center

Studies on the mechanism of catalysis of peptide bond formation by the ribosome have been influenced by high-resolution structures of isolated 50S subunits bound with oligonucleotide analogs of tRNA, including a construct designed to mimic the acceptor ends of the A and P site tRNAs joined together in the transition state of the peptidyl-transferase reaction (Nissen et al., 2000; Schmeing et al., 2005a). These studies have shown that the catalytic site is composed exclusively of RNA, a conclusion that is also supported by our results. Surprisingly few differences were observed for the positions of the 23S rRNA nucleotides of the substrates or the surrounding features of the peptidyl-transferase center (PTC) between the structures of vacant 50S subunits and those of most 50S-substrate complexes or even the *E. coli* 70S ribosome, apart from A2602, whose orientation has been found to be highly variable (Ban et al., 2000; Harms et al., 2001; Schuwirth et al., 2005). The first indications of structural mobility in the PTC come from a more recent study, where it was found that the presence of a CCA-containing A site substrate analog induces conformational shifts of several nucleotides, including U2506, G2583, and U2584-2585 as well as the substrate analog, resulting in exposure of the carbonyl group of the peptidyl substrate to attack by the aminoacyl group (Schmeing et al., 2005b).

In our structure, which represents the first detailed description of the interactions between a full-length P site tRNA and a complete 70S ribosome, the state of our deacylated tRNA is expected to resemble most closely that of a tRNA bound to the P site immediately following peptide bond formation, with the difference that the A site of our complex is not occupied by peptidyl-tRNA. When compared with the structure of an *H. marismortui* 50S complex containing a CCA oligonucleotide bound to the P site (as well as to the A and E sites), our electron density map (Figure 2A) shows significant movement of critical nucleotides in the catalytic site (Figure 2B). It should be kept in mind that the comparisons presented here need to take into account possible phylogenetic structural differences between *T. thermophilus, E. coli*, and *H. marismortui* ribosomes and the effects of different crystal lattice contacts and crystallization conditions on ribosome conformation as well as the different kinds of complexes that were used. Nevertheless, detailed comparison of the structure of the peptidyl-transferase region of our 70S complex with those found for model complexes of the *H. marismortui* 50S subunit and the vacant *E. coli* 70S ribosome shows that, apart from movement of certain specific nucleotides in the PTC, the positions of most nucleotides in the surrounding structure (e.g., C2065 and U2449) are superimposable (Figure 2B).

One of the shifted nucleotides is A2451 (Figures 2B and 2D), previously implicated in the peptidyl-transferase catalytic mechanism because of the proximity of its N3 to a critical oxygen in the bound Yarus transition-state analog (Nissen et al., 2000). In our structure, the N3 of A2451 moves toward the O3′ position of ribose 76, resulting in disruption of the A2451-G2102-G2482 base triple. Coupled with this is a movement of the noncanonical A2450-C2063 base pair and A76 of the P site tRNA toward each other, bringing the A-C pair within H-bonding distance of the 2′OH group of A76 (Figure 2E), which has been shown to play an essential role in catalysis (Dorner et al., 2003; Quiggle et al., 1981; Weinger et al., 2004). This raises the possibility that the A-C pair, which is expected to have a pK_a in the range of 6.0–6.5 (Cai and Tinoco, 1996), acts as a proton donor/acceptor, by analogy with the active-site histidines in many protein enzymes. Studies of the pH-rate dependence of the peptidyl-transferase reaction identified a ribosomal group with an apparent pK_a of ~7.5 (Fahnestock et al., 1970), and it was suggested that this group could be the universally conserved A2450-C2063 wobble pair (Katunin et al., 2002). Replacement of the A2450-C2063 pair by an isosteric but uncharged G-U wobble pair results in loss of the characteristic pK_a as well as a 200-fold or more decrease in the catalytic rate using the puromycin reaction, suggesting that the protonated A-C pair is responsible for the pH-rate dependence and that peptidyl-transferase activity depends on the uncharged (deprotonated) form (Hesslein et al., 2004). However, more recent studies by the same group using a full-length aminoacyl-tRNA as an A site substrate have shown disappearance of the pH-rate dependence in the pH range 6.0 to 9.0, suggesting that the titratable group is important for positioning the model

puromycin substrate and calling into question possible acid-base catalysis by the ribosome (Bieling et al., 2006). One caveat of these experiments is that binding of full-length aminoacyl-tRNA substrate is rate limiting and so could mask changes in rate for the chemical step of the peptidyl-transferase reaction. In a second experiment, where the α-amino group of the aminoacyl-tRNA was replaced by hydroxyl, the pH-rate dependence was also not observed; however, in this case, the rate of the reaction was reduced by >50,000-fold, raising the possibility that details of the catalytic mechanism might differ from those of authentic peptide bond formation. Brunelle et al. (2006) recently showed that use of (5′) C-P puromycin in place of puromycin as A site substrate eliminated the pK_a attributable to the ribosomal structural change, suggesting that base pairing of C75 of the A site substrate with G2553 triggers this change in a way that removes its pH dependence. Although the potential role of the noncanonical A2450-C2063 base pair in the peptidyl-transferase reaction remains an open question, the ability of this critical region of the ribosome to undergo movement needs to be taken into consideration in formulating mechanistic models involving the 50S P site.

The 70S E Site

The E (exit) site binds deacylated tRNA prior to its release from the ribosome and has a virtually absolute specificity for tRNA bearing a free ribose at its acceptor end. Its role is thought to be to provide a favorable free-energy difference for movement of tRNA out of the P site during translocation (Lill et al., 1989; Moazed and Noller, 1989b). Indeed, destabilization of interactions between tRNA and the 50S E site has been found to inhibit translocation, most likely by interfering with formation of the intermediate P/E hybrid state (Feinberg and Joseph, 2001; McGarry et al., 2005). In our complex, the E site of the 70S ribosome is filled by an endogenous tRNA that most likely represents a heterogeneous mixture of tRNA species. Refinement statistics indicate that the E site is fully occupied; although the electron density map is somewhat weaker for its D, T, and anticodon loops, density for the stems of E-tRNA is as strong as that observed for the P-tRNA. The weaker density for the loops and the heterogeneity of the tRNAs in the E site make it difficult to interpret the state of codon-anticodon pairing in the E site, an issue of potential relevance to a proposed reciprocal allosteric interaction between the ribosomal A and E sites (Nierhaus, 1990). A definitive answer to this question will thus have to await the structure of a complex containing a cognate tRNA bound in the E site.

The 70S E site holds the deacylated tRNA by interactions with 16S rRNA, 23S rRNA, and three ribosomal proteins (Table S1). In the 30S subunit, 16S rRNA interacts with the E site ASL exclusively via backbone-backbone interactions, explaining why no E site tRNA footprint was observed for 16S rRNA using base-specific chemical probes (Moazed and Noller, 1986, 1990). Ribose 694 and phosphate 695 pack against phosphate 39 of the E-tRNA anticodon stem, possibly mediated by a magnesium ion, and phosphate 1340 packs on ribose 35 in the anticodon loop. The sole 30S protein interaction is with the C-terminal α helix of protein S7, which contacts the E-tRNA backbone at ribose 41. Guanine 693 of 16S rRNA packs against ribose 1 of the E codon. The previously observed protection of G693 from kethoxal by binding of tRNA or an ASL to the 30S P site (Moazed and Noller, 1986, 1990) is likely due to contact between G693 and the E codon that is induced upon formation of the flanking P site codon-anticodon interaction.

In the 50S subunit, the elbow of E site tRNA contacts both protein L1 and the head of the L1 stalk (helices 76-78) of 23S rRNA, corresponding to a large-scale movement of the stalk relative to the structures of the vacant 70S ribosome (Schuwirth et al., 2005) or the isolated 50S subunit (Harms et al., 2001). Reversal of this movement of the L1 stalk would allow release of the tightly sequestered deacylated tRNA from the ribosome (Figure 3A). Contact between the tRNA and 23S rRNA involves stacking of the tertiary G19-C56 base pair of tRNA on the sheared G2112-A2169 tertiary pair of 23S rRNA (Figure 3B). This interaction accounts for the protection of G2112 and A2169 from chemical probes by E site tRNA (Moazed and Noller, 1989a). Protein L1 contacts the E-tRNA elbow at Ψ55 in the T loop with the tip of the β hairpin around Lys167 and contacts the T stem backbone at positions 61-62 from the end of another β hairpin at Arg52 and Arg53. The contribution of the tRNA elbow contacts to E site binding is clear from the greatly impaired E site binding of ribosomes lacking L1 (L. Hoang and H.F.N., unpublished data).

The minor-groove surface at the end of the acceptor stem of the E-tRNA makes extensive backbone-backbone contacts at nucleotides 70-71 with the minor groove of helix 68 of 23S rRNA (Figure 3C). These include a ribose-zipper interaction (Cate et al., 1996) between the 2′OH of ribose 1851 of 23S rRNA and the base and ribose of G71 of E-tRNA (Figure 3D). The functional importance of this interaction was demonstrated by Feinberg and Joseph (2001), who have shown that methylation of ribose 71 of P site tRNA blocks EF-G-dependent translocation. Since no ribosomal contacts are made with ribose 71 in the 70S P site, inhibition of translocation must be due to the inability of the methylated deacylated tRNA to move from the P/P into the P/E hybrid state. Protein L28 contacts the backbone of the acceptor end of E-tRNA at positions 73 and 74 via basic side chains in its extended β hairpin around residues 38-39 (Figure 4A). Although L33 has been crosslinked to the 3′ adenosine of E-tRNA (Kirillov et al., 2002), we have not yet placed this protein in our structure. Crucial to E site binding is the 3′-terminal adenosine of tRNA, which must be deacylated and unmodified (Feinberg and Joseph, 2001; Lill et al., 1988). In our structure, A76 is recognized and fixed in position by extensive stacking and H-bonding interactions with 23S rRNA (Figure 4A). As in the complex between the *H. marismortui* 50S subunit and a CCA-containing RNA hairpin

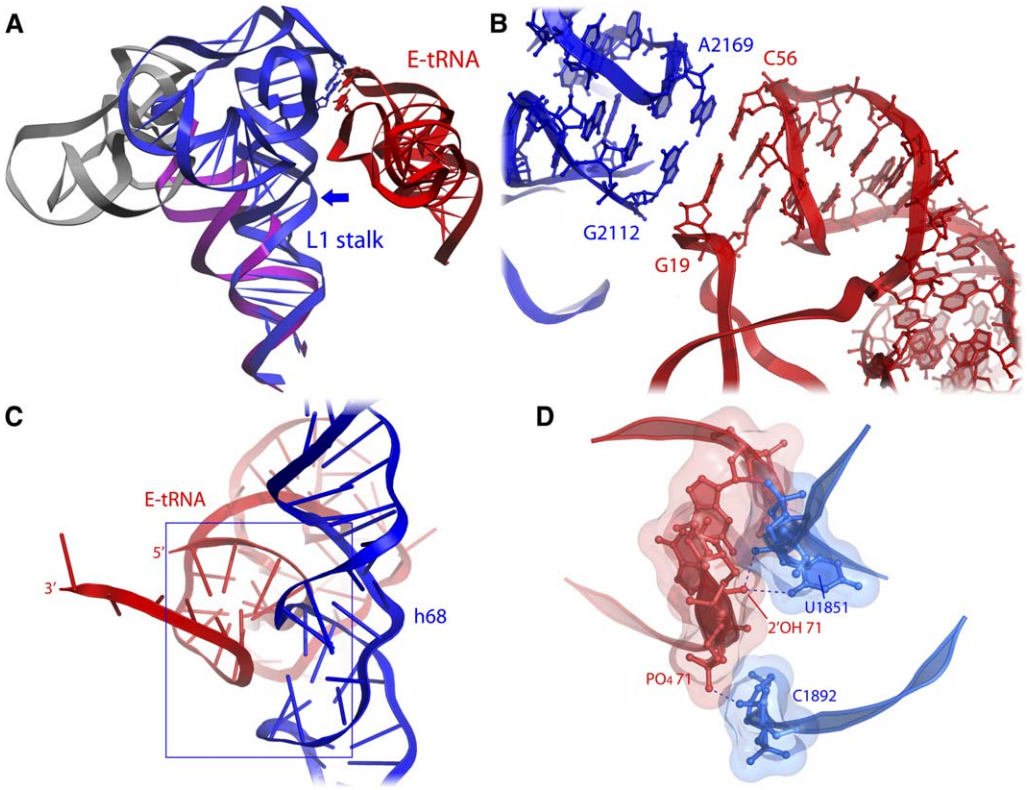

Figure 3. E Site tRNA Interactions

(A) Interaction of the elbow of E site tRNA (red) with 23S rRNA (blue) in the L1 stalk region, showing the large-scale displacement of the stalk relative to its position in the vacant ribosome (Schuwirth et al., 2005) induced by tRNA binding. The blue arrow indicates the extreme compression of the major groove of helix 76 of 23S rRNA that accompanies this movement.

(B) Stacking of the G19-C56 tertiary base pair of tRNA on the G2112-A2169 tertiary pair of 23S rRNA.

(C) Packing of the acceptor stem of E site tRNA (red) against helix 68 of 23S rRNA (blue).

(D) Detailed view of ribose-zipper interactions involving ribose 71 of E site tRNA in the region boxed in (C).

analog of E-tRNA (Schmeing et al., 2003), adenine 76 is rotated away at a 90° angle to the planes of the stacked bases in the acceptor stem, intercalating between bases G2421 and A2422 of 23S rRNA and H bonded to phosphate 2422 (Figures 4A and 4B). Previous biochemical studies have strongly implicated the conserved C2394 in E-tRNA binding. The 2′ hydroxyl of ribose 76 of the deacylated E-tRNA is H bonded to C2394, similarly to that of the 50S model complex, helping to explain the specificity of the E site for deacylated tRNA (Lill et al., 1988), protection of C2394 by E-tRNA (Moazed and Noller, 1989a), and destabilization of E site binding by 2′-O-methylation (Bocchetta et al., 2001) or mutation of C2394 to G (Sergiev et al., 2005). In contrast, the path of the 3′ tail differs markedly between our *T. thermophilus* 70S complex and that observed for the *H. marismortui* 50S complex. In our structure, C74 and C75 are stacked continuously with nucleotide 73 and the acceptor stem (Figure 4A), while in the 50S complex, C75 was flipped out on the opposite side of the backbone, unstacking it from C74, stabilized in part by H bonding of phosphate 76 to the 2′OH of ribose 74 (Figure 4B). These differences are likely due to phylogenetic differences between the structures of the E sites of the ribosomes used in these studies. Although the 23S rRNA elements of the two E sites are nearly identical, contacts with the tail, other than with A76, are made exclusively with proteins. The archaeal *H. marismortui* 50S subunit lacks protein L28 and instead has L44e in the E site, a protein of unrelated sequence or fold (Schmeing et al., 2003). Schmeing et al. also noted that the overall orientation of the stem of their E-tRNA analog differs from that of the full-length E site tRNA as seen in the 5.5 Å structure of the *T. thermophilus* 70S complex and concluded that their analog was most likely bound in a way that resembles the P/E hybrid state, rather than the E/E state, which could also help to account for these differences. A further possibility is that the additional ribosomal contacts made by a full-length tRNA cause it to bind to the E site differently from an acceptor-stem mimic interacting with the isolated 50S subunit.

Distortion of tRNA Structure by the Ribosome

Interaction of tRNA with the ribosome can cause significant conformational changes in tRNA, as illustrated by

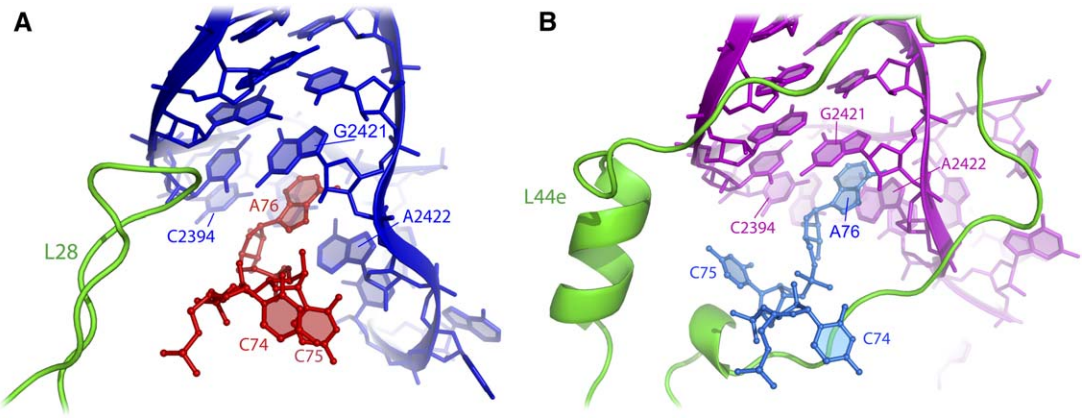

Figure 4. Interactions between the CCA Tail of tRNA and the 50S E Site

Comparison of the binding and conformations of (A) the CCA tail of tRNA to the E site of the *T. thermophilus* 70S complex and (B) a CCA-containing RNA hairpin to the *H. marismortui* 50S E site (Schmeing et al., 2003).

cryo-EM images of the EF-Tu ternary complex bound to the ribosome (Valle et al., 2003). In that study, tRNA was visualized both in the A/T state, bound to the ribosome in complex with EF-Tu, and in the A/A state. In the A/T state, the anticodon arm of the tRNA is bent by more than 30° to allow initial codon recognition, while in the A/A state, the tRNA is bent by about 15°. The hinge point was localized to the junction of the anticodon and D stems at or near the purine-purine base pair between positions 26 and 44.

Our structure shows that binding of tRNA to the ribosomal P and E sites causes significant distortion of the structure of tRNA when compared to the 2.0 Å crystal structure of yeast $tRNA^{Phe}$ (Jovine et al., 2000), which was used as the initial model for our refinements. Root-mean-square differences (rmsds) between backbone phosphorus atoms of P- and E-tRNA with respect to those of yeast $tRNA^{Phe}$ are 2.1 and 2.0 respectively. Both tRNAs are kinked at the junction of the anticodon and D stems, centered on the A26-G44 purine-purine base pair, bending the body of the tRNA relative to the ASL (Figures 5A–5D). Kinking of the P-tRNA is most pronounced, causing it to bend toward the large subunit by about 10° (Figure 5B). In addition, there is a partial unwinding of the D stem relative to the anticodon stem, resulting in a rotation of the body of the P-tRNA relative to the ASL by about 10° around the axis of the anticodon stem, orienting it slightly toward the A site (Figure 5A). The body of the E-tRNA also rotates by about 10° relative to the ASL, but around an axis drawn between the 26-44 base pair and its 3′ acceptor end, moving its elbow in the direction of the L1 stalk (Figures 5C and 5D). Interestingly, kinking has been observed to be most extreme in the A/T state, decreasing incrementally as the tRNA passes from the A/T through the A/A, P/P, and E/E states. If kinking represents a higher-energy state than the free state, as suggested by previous studies (Auffinger et al., 1999; Ehrenberg et al., 1979; Friederich et al., 1998), the energy to drive tRNA movement might derive in part from gradual relaxation of the conformational energy introduced in the initial A/T binding state by EF-Tu and GTP (Valle et al., 2003). Another notable change is seen in the anticodon loops, as suggested by our previous 5.5 Å structure (Yusupov et al., 2001); the P-tRNA anticodon loop is wider and more rounded than that of the isolated tRNA, while the apex of the E-tRNA loop is narrow and more sharply kinked (Figure 5E).

Conformational Differences between Different Ribosome Structures

Several large-scale rearrangements are revealed by comparison of the structure from the present crystal form with the previous 5.5 Å structure of a similar *T. thermophilus* tRNA-mRNA-ribosome complex (Yusupov et al., 2001). The rmsds for backbone phosphorus atoms of the 30S and the 50S subunits between ribosomes from the two crystal forms are 2.2 and 2.5 Å, respectively. If the two structures are superimposed on their 23S rRNAs, it can be seen that, in our model, both the head and body of the small subunit move relative to the large subunit (data not shown). Viewed from the interface, the head rotates counterclockwise and the body clockwise, each by about 2°, around an axis perpendicular to the interface plane, closing the gap between the head and shoulder at 16S rRNA nucleotides 422 and 1045 by ~5 Å. At the same time, the top of the head moves toward the 50S subunit by about 4 Å. In the 50S subunit, the C-terminal domain of L9, which makes a crystal contact with the 30S subunit of a symmetry mate, is displaced by about 10 Å downward, away from the L1 stalk.

Changes in ribosome structure in response to tRNA binding are suggested by comparison of our structure with that of the vacant 70S ribosome (Schuwirth et al., 2005). Our comparison is made with *E. coli* structure I, whose structure is most similar to ours (Schuwirth et al., 2005). Since both structures come from eubacterial ribosomes, in addition to the fact that structural features

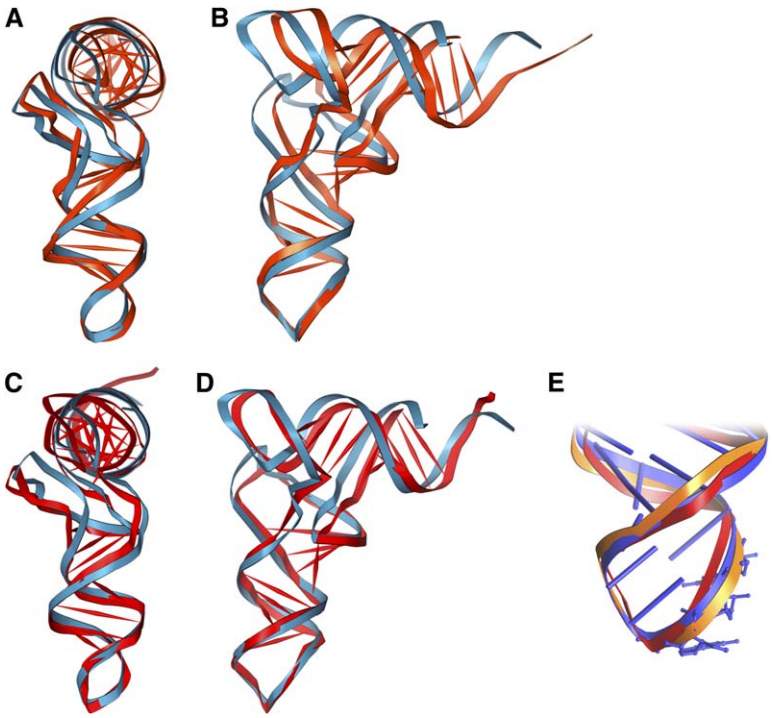

Figure 5. Distortion of tRNA Structure in the P and E Sites

(A and B) P-tRNA.

(C and D) E-tRNA.

(E) Anticodon loop deformations showing the differences between the loop conformations of P-tRNA (orange), E-tRNA (red), and the crystal structure of free $tRNA^{Phe}$ (Jovine et al., 2000).

involved in ribosomal function are often universally conserved, many functionally relevant conformational changes are unlikely to be due to species differences. Differences between the tRNA-ribosome complexes and vacant ribosomes are even more pronounced (rmsd values for the 30S and 50S subunits of 3.0 and 2.6 Å, respectively). In the 30S subunit (Figure 6A), the most prominent difference is seen for the head of the subunit, which moves as a rigid body (Schuwirth et al., 2005), pivoting around the neck (helix 27 of 16S rRNA) such that top of the head undergoes a movement of about 15 Å. As a result, the 1240 and 1340 regions of 16S rRNA clash strongly with the positions of the P- and E-tRNAs, as seen in our structure (Figure 6C). This particular difference is unlikely to be attributable simply to the presence or absence of tRNA since cryo-EM reconstructions of vacant ribosomes do not appear to undergo such movement (Frank and Agrawal, 2000). Elsewhere in the small subunit, localized differences are seen for individual helices, including the "spur" (helix 6), helix 23 in the right-hand side of the platform, and in the middle of the penultimate stem (helix 44). The latter difference is especially interesting because of its location close to the axis of rotation for the relative movement of the 30S and 50S subunits (Gao et al., 2003) and because of the apparent localized mobility of the middle of the penultimate stem.

In the 50S subunit, the most dramatic conformational difference is found in the L1 stalk, which is displaced by about 30 Å away from the P site in the vacant ribosome, reflecting a movement that is most likely coupled to release of tRNA from the E site. It opens even further in the free 50S subunit (Harms et al., 2001), pivoting around nucleotides G2100-U2189 of helix 76 by 30° with respect to the structure of the 70S complex, resulting in displacement of the top of the L1 stalk by about 40 Å (Figure 3A and Figure 6B). Movement of the L1 stalk between all three structures can be ascribed to a localized flexibility between nucleotides 2187-2193 and 2096-2102. The major groove of this part of helix 76 is dramatically compressed in the 70S functional complex (Figure 3A), where the L1 stalk moves toward the interface to contact the elbow of E site tRNA, as discussed above. The distorted region is rich in G-U wobble pairs, which are present in nearly all species. The presence of G-U pairs in double helices has been shown to increase their deformability (Chang et al., 1999; Ramos and Varani, 1997), in this case enabling large-scale movement of the L1 stalk.

Structural differences are also observed between our structure and the *E. coli* structure in the interactions forming two of the dozen intersubunit bridges that are responsible for joining the 30S and 50S subunits. These are of interest because of their role in enabling the intersubunit movement that occurs during the translocation step of protein synthesis (Gao et al., 2003). The RNA and protein components of the bridges were first identified in lower-resolution crystal structures of *T. thermophilus* 70S ribosomes (Cate et al., 1999; Culver et al., 1999; Yusupov et al., 2001) and described in detail for the *E. coli* structures (Schuwirth et al., 2005). The bridges in the structure presented here are very similar in detail to those described by Schuwirth et al., with the exception of bridges B1a and B1b, which can be explained by the different positions of the head in the three structures. In bridge B1a, which connects protein S13 in the head of the 30S subunit with the

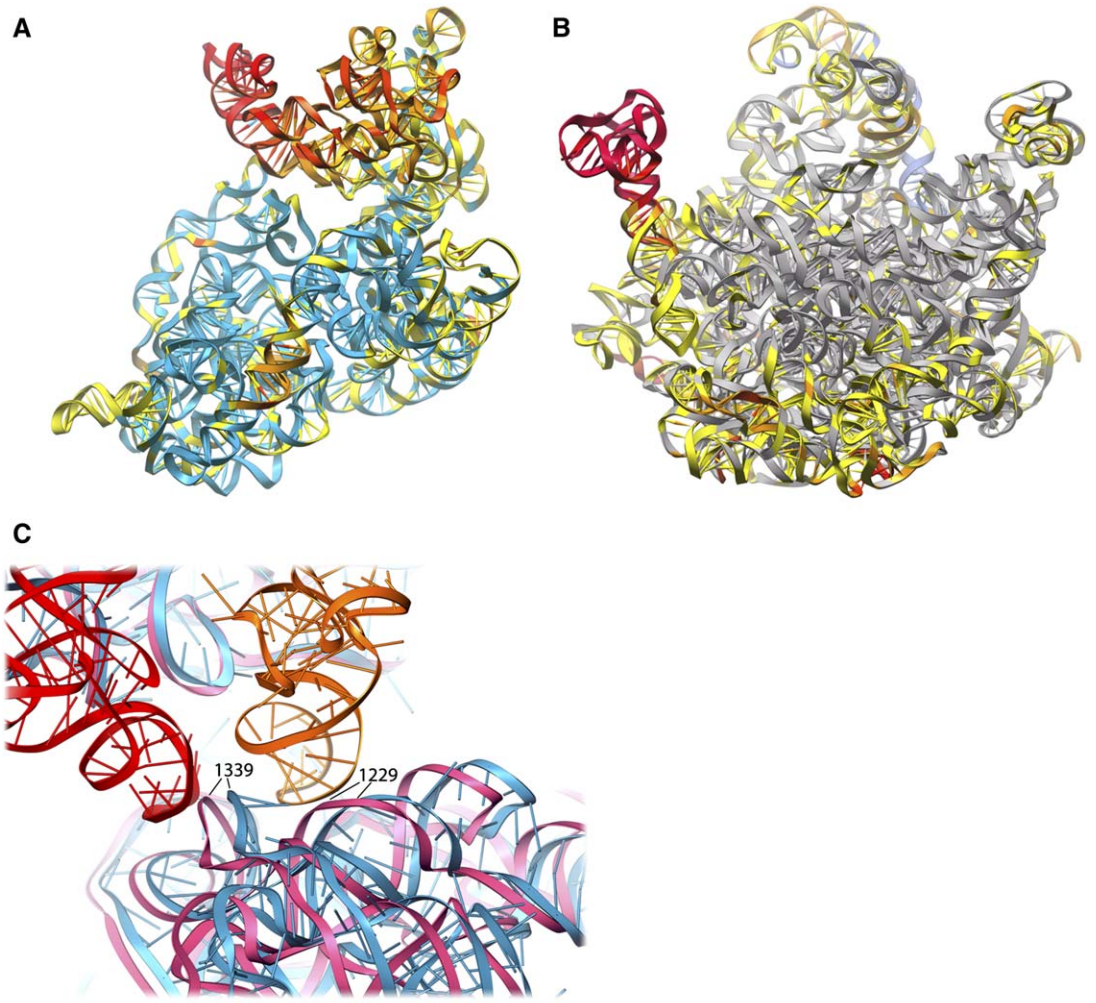

Figure 6. Conformational Variations between Different Ribosome Crystal Structures

(A and B) Comparison of (A) 16S and (B) 23S rRNAs in vacant *E. coli* (Schuwirth et al., 2005) and tRNA-occupied *T. thermophilus* ribosomes (this work). Colors indicate the rmsd values for individual nucleotides between the two structures: 0–2 Å, cyan (16S rRNA) or gray (23S rRNA); 2–4 Å, yellow; 4–7 Å, gold; 7–10 Å, orange; 10–14 Å, red; >14 Å, magenta.

(C) Comparison of the positions of features of the 3′ major domain of 16S rRNA between the vacant *E. coli* 70S ribosome (magenta) (Schuwirth et al., 2005) and the *T. thermophilus* tRNA-containing complex (cyan), showing clash between the 16S rRNA in the *E. coli* structure with P-tRNAs (orange) and E-tRNAs (red) from the *T. thermophilus* complex.

A site finger (helix 38) of 23S rRNA and is disordered in both *E. coli* structures, nucleotides 886-888 of 23S rRNA make two separate contacts with S13 at positions 79-83 and 93-94. Bridge B1b, which connects the head of the 30S subunit with the central protuberance of the 50S subunit via interactions between proteins S13 and L5, takes two different forms in the two *E. coli* structures (Schuwirth et al., 2005). Our structure has a third form (data not shown), in which three different regions of S13 contact L5, none of which are the same as those observed in the *E. coli* structures.

Conclusion

The increased resolution of this 70S ribosome complex provides a greatly enhanced view of the details of ribosome-tRNA interactions in the P and E sites. We can now account for the high degree of phylogenetic conservation of many of the features of ribosomes and tRNA, and particularly how the unique structural capabilities of RNA are exploited to create a functional ribosome. Our structure also presents new evidence that both the ribosome and its RNA substrates are exquisitely dynamic molecules whose structural rearrangements are an integral part of the mechanism of protein synthesis. In spite of the rapid progress from structural, biochemical, biophysical, and genetic studies of ribosomes during recent years, we nevertheless lack a full understanding of the mechanisms of the fundamental processes of tRNA selection and accommodation, translocation, and catalysis of peptide bond formation, not to mention many other important

functions. A detailed, static structure of a ribosome complex is thus only a starting point for future studies that will ultimately need to explain the molecular dynamics of translation at atomic resolution.

EXPERIMENTAL PROCEDURES

Ribosomes were purified from *Thermus thermophilus* cells and crystallized as described in the Supplemental Experimental Procedures. Diffraction data were collected at beamline 12.3.1 at the Advanced Light Source at Lawrence Berkeley National Laboratory using an X-ray wavelength of 1.115879 Å and an oscillation angle of 0.25°. They were integrated with D*TREK (Pflugrath, 1999) and scaled with SCALA (Evans, 2006). An all-atom energy-minimized model of the 70S *T. Thermophilus* ribosome (Tung and Sanbonmatsu, 2004) was used as a starting structure, with some modifications. Large-subunit ribosomal protein models for L16, L18, L23, and L27 were added or replaced with the structures of *T. Thermophilus* proteins determined recently by X-ray crystallography and NMR (Nishimura et al., 2004; Ohman et al., 2003; Wang et al., 2004; Woestenenk et al., 2002). Initial protein models with unknown three-dimensional structures were obtained by sequence alignment against homologous structures using T-COFFEE (Notredame et al., 2000) and subsequent homology modeling using Modeller (Fiser and Sali, 2003). The 2.0 Å yeast $tRNA^{Phe}$ structure (Jovine et al., 2000) was used as the starting model for P and E site tRNAs. Molecular replacement and reciprocal-space torsion-angle simulated annealing refinements were performed with CNS (Brünger et al., 1998). O (Jones et al., 1991) and PyMOL (http://pymol.sourceforge.net/) were used for manual refitting against composite omit $2F_o - F_c$ maps. Stereochemically restrained real-space refinement of refitted regions as well as of the entire model was carried out using RSRef2000 (Korostelev et al., 2002). Composite omit maps calculated using CNS (Brünger et al., 1998) were used to minimize the effect of model bias (Hodel et al., 1992). Refinement of TLS parameters was performed using REFMAC (Winn et al., 2003) at the final stage of structure determination and led to R/R_{free} of 0.346/0.347. The resolution limit of 3.7 Å was initially determined empirically by improvement in the quality of the electron density map and was confirmed statistically with the crossvalidated σ_A method of Ling et al. (1998) as used by DeLaBarre and Brünger (2006) (Figure S2). Absence of strong model bias is evident from the poor fit of the starting model to the electron density map (Figure S3). Superposition of structures and calculation of rmsd values were performed in PyMOL. Figures were rendered using PyMOL and Ribbons (Carson, 1997).

Supplemental Data

Supplemental Data include Supplemental Experimental Procedures, three figures, and one table and can be found with this article online at http://www.cell.com/cgi/content/full/126/6/1065/DC1/.

ACKNOWLEDGMENTS

We thank W.G. Scott, A. Baucom, L. Lancaster, H. Asahara, C. Spiegel, and J. Nix for their help at various stages of this work; C. Gorringe for computational support and rendering of figures; C. Chan for support at the UCB fermentation facility; and J. McCloskey for sharing his unpublished posttranscriptional modification results. This work was supported by grants from the NIH and the Agouron Institute and a fellowship from the Danish Research Council to M.L. Beamline 12.3.1 at the ALS is supported by grants from the NIH and the US Department of Energy.

Received: July 13, 2006
Revised: August 10, 2006
Accepted: August 30, 2006
Published online: September 7, 2006

REFERENCES

Agrawal, R.K., Heagle, A.B., Penczek, P., Grassucci, R.A., and Frank, J. (1999). EF-G-dependent GTP hydrolysis induces translocation accompanied by large conformational changes in the 70S ribosome. Nat. Struct. Biol. *6*, 643–647.

Auffinger, P., Louise-May, S., and Westhof, E. (1999). Molecular dynamics simulations of solvated yeast tRNA(Asp). Biophys. J. *76*, 50–64.

Ban, N., Nissen, P., Hansen, J., Moore, P.B., and Steitz, T.A. (2000). The complete atomic structure of the large ribosomal subunit at 2.4 Å resolution. Science *289*, 905–920.

Bieling, P., Beringer, M., Adio, S., and Rodnina, M.V. (2006). Peptide bond formation does not involve acid-base catalysis by ribosomal residues. Nat. Struct. Mol. Biol. *13*, 423–428.

Bocchetta, M., Xiong, L., Shah, S., and Mankin, A.S. (2001). Interactions between 23S rRNA and tRNA in the ribosomal E site. RNA *7*, 54–63.

Brodersen, D.E., Clemons, W.M., Jr., Carter, A.P., Morgan-Warren, R.J., Wimberly, B.T., and Ramakrishnan, V. (2000). The structural basis for the action of the antibiotics tetracycline, pactamycin, and hygromycin B on the 30S ribosomal subunit. Cell *103*, 1143–1154.

Brunelle, J.L., Youngman, E.M., Sharma, D., and Green, R. (2006). The interaction between C75 of tRNA and the A loop of the ribosome stimulates peptidyl transferase activity. RNA *12*, 33–39.

Brünger, A.T., Adams, P.D., Clore, G.M., DeLano, W.L., Gros, P., Grosse-Kunstleve, R.W., Jiang, J.S., Kuszewski, J., Nilges, M., Pannu, N.S., et al. (1998). Crystallography & NMR system: A new software suite for macromolecular structure determination. Acta Crystallogr. D Biol. Crystallogr. *54*, 905–921.

Cai, Z., and Tinoco, I., Jr. (1996). Solution structure of loop A from the hairpin ribozyme from tobacco ringspot virus satellite. Biochemistry *35*, 6026–6036.

Carson, M. (1997). Ribbons. Methods Enzymol. *277B*, 493–505.

Cate, J.H., Gooding, A.R., Podell, E., Zhou, K., Golden, B.L., Szewczak, A.A., Kundrot, C.E., Cech, T.R., and Doudna, J.A. (1996). RNA tertiary structure mediation by adenosine platforms. Science *273*, 1696–1699.

Cate, J.H., Yusupov, M.M., Yusupova, G.Z., Earnest, T.N., and Noller, H.F. (1999). X-ray crystal structures of 70S ribosome functional complexes. Science *285*, 2095–2104.

Chang, K.Y., Varani, G., Bhattacharya, S., Choi, H., and McClain, W.H. (1999). Correlation of deformability at a tRNA recognition site and aminoacylation specificity. Proc. Natl. Acad. Sci. USA *96*, 11764–11769.

Culver, G.M., Cate, J.H., Yusupova, G.Z., Yusupov, M.M., and Noller, H.F. (1999). Identification of an RNA-protein bridge spanning the ribosomal subunit interface. Science *285*, 2133–2136.

Dallas, A., and Noller, H.F. (2001). Interaction of translation initiation factor 3 with the 30S ribosomal subunit. Mol. Cell *8*, 855–864.

DeLaBarre, B., and Brünger, A.T. (2006). Considerations for the refinement of low-resolution crystal structures. Acta Crystallogr. D Biol. Crystallogr. *62*, 923–932.

Dorner, S., Panuschka, C., Schmid, W., and Barta, A. (2003). Mononucleotide derivatives as ribosomal P-site substrates reveal an important contribution of the 2′-OH to activity. Nucleic Acids Res. *31*, 6536–6542.

Ehrenberg, M., Rigler, R., and Wintermeyer, W. (1979). On the structure and conformational dynamics of yeast phenylalanine-accepting transfer ribonucleic acid in solution. Biochemistry *18*, 4588–4599.

Evans, P. (2006). Scaling and assessment of data quality. Acta Crystallogr. D Biol. Crystallogr. *62*, 72–82.

Fahnestock, S., Neumann, H., Shashoua, V., and Rich, A. (1970). Ribosome-catalyzed ester formation. Biochemistry *9*, 2477–2483.

Feinberg, J., and Joseph, S. (2001). Identification of molecular interactions between P site tRNA and the ribosome essential for tanslocation. Proc. Natl. Acad. Sci. USA *98*, 11120–11125.

Fiser, A., and Sali, A. (2003). Modeller: generation and refinement of homology-based protein structure models. Methods Enzymol. *374*, 461–491.

Frank, J., and Agrawal, R.K. (2000). A ratchet-like inter-subunit reorganization of the ribosome during translocation. Nature *406*, 318–322.

Friederich, M.W., Vacano, E., and Hagerman, P.J. (1998). Global flexibility of tertiary structure in RNA: yeast tRNAPhe as a model system. Proc. Natl. Acad. Sci. USA *95*, 3572–3577.

Gao, H., Sengupta, J., Valle, M., Korostelev, A., Eswar, N., Stagg, S.M., Van Roey, P., Agrawal, R.K., Harvey, S.C., Sali, A., et al. (2003). Study of the structural dynamics of the E coli 70S ribosome using real-space refinement. Cell *113*, 789–801.

Green, R., and Noller, H.F. (1997). Ribosomes and Translation. Annu. Rev. Biochem. *66*, 679–716.

Guymon, R., Pomerantz, S.C., Crain, P.F., and McCloskey, J.A. (2006). Influence of phylogeny on posttranscriptional modification of rRNA in thermophilic prokaryotes: the complete modification map of 16S rRNA of Thermus thermophilus. Biochemistry *45*, 4888–4899.

Hansen, J.L., Ippolito, J.A., Ban, N., Nissen, P., Moore, P.B., and Steitz, T.A. (2002). The structures of four macrolide antibiotics bound to the large ribosomal subunit. Mol. Cell *10*, 117–128.

Harms, J., Schluenzen, F., Zarivach, R., Bashan, A., Gat, S., Agmon, I., Bartels, H., Franceschi, F., and Yonath, A. (2001). High resolution structure of the large ribosomal subunit from a mesophilic eubacterium. Cell *107*, 679–688.

Hesslein, A.E., Katunin, V.I., Beringer, M., Kosek, A.B., Rodnina, M.V., and Strobel, S.A. (2004). Exploration of the conserved A+C wobble pair within the ribosomal peptidyl transferase center using affinity purified mutant ribosomes. Nucleic Acids Res. *32*, 3760–3770.

Hodel, A., Kim, S.-H., and Brünger, A.T. (1992). Model bias in macromolecular crystal structures. Acta Crystallogr. *A48*, 851–858.

Jenner, L., Romby, P., Rees, B., Schulze-Briese, C., Springer, M., Ehresmann, C., Ehresmann, B., Moras, D., Yusupova, G., and Yusupov, M. (2005). Translational operator of mRNA on the ribosome: how repressor proteins exclude ribosome binding. Science *308*, 120–123.

Jones, T.A., Zou, J.Y., Cowan, S.W., and Kjeldgaard. (1991). Improved methods for binding protein models in electron density maps and the location of errors in these models. Acta Crystallogr. A *47*, 110–119.

Jovine, L., Djordjevic, S., and Rhodes, D. (2000). The crystal structure of yeast phenylalanine tRNA at 2.0 A resolution: cleavage by Mg(2+) in 15-year old crystals. J. Mol. Biol. *301*, 401–414.

Katunin, V.I., Muth, G.W., Strobel, S.A., Wintermeyer, W., and Rodnina, M.V. (2002). Important contribution to catalysis of peptide bond formation by a single ionizing group within the ribosome. Mol. Cell *10*, 339–346.

Kirillov, S.V., Wower, J., Hixson, S.S., and Zimmermann, R.A. (2002). Transit of tRNA through the Escherichia coli ribosome: cross-linking of the 3′ end of tRNA to ribosomal proteins at the P and E sites. FEBS Lett. *514*, 60–66.

Korostelev, A., Bertram, R., and Chapman, M.S. (2002). Simulated-annealing real-space refinement as a tool in model building. Acta Crystallogr. D Biol. Crystallogr. *58*, 761–767.

Lancaster, L., and Noller, H.F. (2005). Involvement of 16S rRNA nucleotides G1338 and A1339 in discrimination of initiator tRNA. Mol. Cell *20*, 623–632.

Lill, R., Lepier, A., Schwagele, F., Sprinzl, M., Vogt, H., and Wintermeyer, W. (1988). Specific recognition of the 3′-terminal adenosine of tRNAPhe in the exit site of Escherichia coli ribosomes. J. Mol. Biol. *203*, 699–705.

Lill, R., Robertson, J.M., and Wintermeyer, W. (1989). Binding of the 3′ terminus of tRNA to 23S rRNA in the ribosomal exit site actively promotes translocation. EMBO J. *8*, 3933–3938.

Ling, H., Boodhoo, A., Hazes, B., Cummings, M.D., Armstrong, G.D., Brunton, J.L., and Read, R.J. (1998). Structure of the shiga-like toxin I B-pentamer complexed with an analogue of its receptor Gb3. Biochemistry *37*, 1777–1788.

McGarry, K.G., Walker, S.E., Wang, H., and Fredrick, K. (2005). Destabilization of the P site codon-anticodon helix results from movement of tRNA into the P/E hybrid state within the ribosome. Mol. Cell *20*, 613–622.

Moazed, D., and Noller, H.F. (1986). Transfer RNA shields specific nucleotides in 16S ribosomal RNA from attack by chemical probes. Cell *47*, 985–994.

Moazed, D., and Noller, H.F. (1989a). Interaction of tRNA with 23S rRNA in the ribosomal A, P, and E sites. Cell *57*, 585–597.

Moazed, D., and Noller, H.F. (1989b). Intermediate states in the movement of transfer RNA in the ribosome. Nature *342*, 142–148.

Moazed, D., and Noller, H.F. (1990). Binding of tRNA to the ribosomal A and P sites protects two distinct sets of nucleotides in 16S rRNA. J. Mol. Biol. *211*, 135–145.

Moazed, D., and Noller, H.F. (1991). Sites of interaction of the CCA end of peptidyl-tRNA with 23S rRNA. Proc. Natl. Acad. Sci. USA *88*, 3725–3728.

Nierhaus, K.H. (1990). The allosteric three-site model for the ribosomal elongation cycle: features and future. Biochemistry *29*, 4997–5008.

Nishimura, M., Yoshida, T., Shirouzu, M., Terada, T., Kuramitsu, S., Yokoyama, S., Ohkubo, T., and Kobayashi, Y. (2004). Solution structure of ribosomal protein L16 from Thermus thermophilus HB8. J. Mol. Biol. *344*, 1369–1383.

Nissen, P., Hansen, J., Ban, N., Moore, P.B., and Steitz, T.A. (2000). The structural basis of ribosome activity in peptide bond synthesis. Science *289*, 920–930.

Noller, H.F., Hoffarth, V., and Zimniak, L. (1992). Unusual resistance of peptidyl transferase to protein extraction procedures. Science *256*, 1416–1419.

Notredame, C., Higgins, D.G., and Heringa, J. (2000). T-Coffee: A novel method for fast and accurate multiple sequence alignment. J. Mol. Biol. *302*, 205–217.

Ogle, J.M., Brodersen, D.E., Clemons, W.M., Tarry, M.J., Carter, A.P., and Ramakrishnan, V. (2001). Recognition of cognate transfer RNA by the 30S ribosomal subunit. Science *292*, 897–902.

Ogle, J.M., Murphy, F.V., Tarry, M.J., and Ramakrishnan, V. (2002). Selection of tRNA by the ribosome requires a transition from an open to a closed form. Cell *111*, 721–732.

Ohman, A., Rak, A., Dontsova, M., Garber, M.B., and Hard, T. (2003). NMR structure of the ribosomal protein L23 from Thermus thermophilus. J. Biomol. NMR *26*, 131–137.

Petry, S., Brodersen, D.E., Murphy, F.V., 4th, Dunham, C.M., Selmer, M., Tarry, M.J., Kelley, A.C., and Ramakrishnan, V. (2005). Crystal structures of the ribosome in complex with release factors RF1 and RF2 bound to a cognate stop codon. Cell *123*, 1255–1266.

Pflugrath, J.W. (1999). The finer things in X-ray diffraction data collection. Acta Crystallogr. D Biol. Crystallogr. *55*, 1718–1725.

Pioletti, M., Schlunzen, F., Harms, J., Zarivach, R., Gluhmann, M., Avila, H., Bashan, A., Bartels, H., Auerbach, T., Jacobi, C., et al. (2001). Crystal structures of complexes of the small ribosomal subunit with tetracycline, edeine and IF3. EMBO J. *20*, 1829–1839.

Prince, J.B., Taylor, B.H., Thurlow, D.L., Ofengand, J., and Zimmermann, R.A. (1982). Covalent crosslinking of tRNA1Val to 16S RNA at the ribosomal P site: identification of crosslinked residues. Proc. Natl. Acad. Sci. USA *79*, 5450–5454.

Quiggle, K., Kumar, G., Ott, T.W., Ryu, E.K., and Chladek, S. (1981). Donor site of ribosomal peptidyltransferase: investigation of substrate specificity using 2′(3′)-O-(N-acylaminoacyl)dinucleoside phosphates as models of the 3′ terminus of N-acylaminoacyl transfer ribonucleic acid. Biochemistry *20*, 3480–3485.

Ramos, A., and Varani, G. (1997). Structure of the acceptor stem of Escherichia coli tRNA Ala: role of the G3.U70 base pair in synthetase recognition. Nucleic Acids Res. *25*, 2083–2090.

Schmeing, T.M., Seila, A.C., Hansen, J.L., Freeborn, B., Soukup, J.K., Scaringe, S.A., Strobel, S.A., Moore, P.B., and Steitz, T.A. (2002). A pre-translocational intermediate in protein synthesis observed in crystals of enzymatically active 50S subunits. Nat. Struct. Biol. *9*, 225–230.

Schmeing, T.M., Moore, P.B., and Steitz, T.A. (2003). Structures of deacylated tRNA mimics bound to the E site of the large ribosomal subunit. RNA *9*, 1345–1352.

Schmeing, T.M., Huang, K.S., Kitchen, D.E., Strobel, S.A., and Steitz, T.A. (2005a). Structural insights into the roles of water and the 2′ hydroxyl of the P site tRNA in the peptidyl transferase reaction. Mol. Cell *20*, 437–448.

Schmeing, T.M., Huang, K.S., Strobel, S.A., and Steitz, T.A. (2005b). An induced-fit mechanism to promote peptide bond formation and exclude hydrolysis of peptidyl-tRNA. Nature *438*, 520–524.

Schuwirth, B.S., Borovinskaya, M.A., Hau, C.W., Zhang, W., Vila-Sanjurjo, A., Holton, J.M., and Cate, J.H. (2005). Structures of the bacterial ribosome at 3.5 A resolution. Science *310*, 827–834.

Sergiev, P.V., Lesnyak, D.V., Kiparisov, S.V., Burakovsky, D.E., Leonov, A.A., Bogdanov, A.A., Brimacombe, R., and Dontsova, O.A. (2005). Function of the ribosomal E-site: a mutagenesis study. Nucleic Acids Res. *33*, 6048–6056.

Stark, H., Rodnina, M.V., Wieden, H.J., van Heel, M., and Wintermeyer, W. (2000). Large-scale movement of elongation factor G and extensive conformational change of the ribosome during translocation. Cell *100*, 301–309.

Tung, C.S., and Sanbonmatsu, K.Y. (2004). Atomic model of the Thermus thermophilus 70S ribosome developed in silico. Biophys. J. *87*, 2714–2722.

Valle, M., Zavialov, A., Li, W., Stagg, S.M., Sengupta, J., Nielsen, R.C., Nissen, P., Harvey, S.C., Ehrenberg, M., and Frank, J. (2003). Incorporation of aminoacyl-tRNA into the ribosome as seen by cryo-electron microscopy. Nat. Struct. Biol. *10*, 899–906.

von Ahsen, U., and Noller, H.F. (1995). Identification of bases in 16S rRNA essential for tRNA binding at the 30S ribosomal P site. Science *267*, 234–237.

Wang, H., Takemoto, C.H., Murayama, K., Sakai, H., Tatsuguchi, A., Terada, T., Shirouzu, M., Kuramitsu, S., and Yokoyama, S. (2004). Crystal structure of ribosomal protein L27 from Thermus thermophilus HB8. Protein Sci. *13*, 2806–2810.

Weinger, J.S., Parnell, K.M., Dorner, S., Green, R., and Strobel, S.A. (2004). Substrate-assisted catalysis of peptide bond formation by the ribosome. Nat. Struct. Mol. Biol. *11*, 1101–1106.

Weiss, M.S. (2001). Global indicators of X-ray data quality. J. Appl. Crystallogr. *34*, 130–135.

Wilson, D.N., Schluenzen, F., Harms, J.M., Yoshida, T., Ohkubo, T., Albrecht, R., Buerger, J., Kobayashi, Y., and Fucini, P. (2005). X-ray crystallography study on ribosome recycling: the mechanism of binding and action of RRF on the 50S ribosomal subunit. EMBO J. *24*, 251–260.

Wimberly, B.T., Brodersen, D.E., Clemons, W.M., Jr., Morgan-Warren, R.J., Carter, A.P., Vonrhein, C., Hartsch, T., and Ramakrishnan, V. (2000). Structure of the 30S ribosomal subunit. Nature *407*, 327–339.

Winn, M.D., Murshudov, G.N., and Papiz, M.Z. (2003). Macromolecular TLS refinement in REFMAC at moderate resolutions. Methods Enzymol. *374*, 300–321.

Woestenenk, E.A., Gongadze, G.M., Shcherbakov, D.V., Rak, A.V., Garber, M.B., Hard, T., and Berglund, H. (2002). The solution structure of ribosomal protein L18 from Thermus thermophilus reveals a conserved RNA-binding fold. Biochem. J. *363*, 553–561.

Yusupov, M., Yusupova, G., Baucom, A., Lieberman, K., Earnest, T.N., Cate, J.H., and Noller, H.F. (2001). Crystal Structure of the Ribosome at 5.5 Å Resolution. Science *292*, 883–896.

Yusupova, G.Z., Yusupov, M., Cate, J.H.D., and Noller, H.F. (2001). The Path of Messenger RNA Through the Ribosome. Cell *106*, 233–241.

Accession Numbers

Coordinates and structure factors reported herein have been deposited in the Protein Data Bank with the ID codes 2I1C and 1VS9.